JGR Atmospheres

RESEARCH ARTICLE
10.1029/2022JD036994

Key Points:

- Two-week persistent Ural blocking (UB) anomalies induce a weaker polar vortex and negative North Atlantic Oscillation
- Role of Barents-Kara (BK) sea ice is secondary compared to the influence of UB
- However, BK sea ice modulates the persistence of the response to UB

Supporting Information:

Supporting Information may be found in the online version of this article.

Correspondence to:

Y. Peings,
ypeings@uci.edu

Citation:

Peings, Y., Davini, P., & Magnusdottir, G. (2023). Impact of Ural blocking on early winter climate variability under different Barents-Kara sea ice conditions. *Journal of Geophysical Research: Atmospheres*, *128*, e2022JD036994. https://doi.org/10.1029/2022JD036994

Received 23 APR 2022
Accepted 27 FEB 2023

Impact of Ural Blocking on Early Winter Climate Variability Under Different Barents-Kara Sea Ice Conditions

Y. Peings[1], P. Davini[2], and G. Magnusdottir[1]

[1]Department of Earth System Science, University of California Irvine, Irvine, CA, USA, [2]Istituto di Scienze dell'Atmosfera e del Clima, Consiglio Nazionale delle Ricerche, Torino, Italy

Abstract Ural blocking (UB) is a prominent mode of variability of the Northern Hemisphere atmospheric circulation, particularly in fall. It can persist for several days and exert a lagged influence on the wintertime NH circulation, providing predictability at the subseasonal time scale. Using two atmospheric models, we explore how the early winter atmospheric circulation responds to a 2-week persistent UB anomaly imposed in early November. Experiments are carried out with two different configurations of Barents-Kara (BK) sea-ice concentration to examine whether it plays a role in how UB impacts atmospheric variability. In both models, the UB anomaly is followed by a weakening of the stratospheric polar vortex and a negative phase of the North Atlantic Oscillation (NAO), which lasts up to 2 months after the forcing is released. Interestingly, the response is more persistent under low BK sea-ice conditions, that is, BK sea ice modulates the atmospheric response to UB. Additional experiments with prescribed sea ice concentration anomalies alone suggest that BK sea ice exerts a limited influence on early winter NH atmospheric variability. The response to UB involves a weakening of the polar vortex that persists longer under low BK sea ice, which explains the more persistent response in that configuration. Our study highlights that UB variability in November is a robust precursor for early winter NAO/polar stratosphere anomalies, and this may be more relevant in the context of declining Arctic sea-ice extent. Provided that climate models accurately capture this teleconnection, it has the potential to improve subseasonal predictions of the NH wintertime climate.

Plain Language Summary Predicting subseasonal fluctuations of the polar stratosphere in winter (or polar vortex) is critical to anticipate weather extreme events over populated areas of the Northern Hemisphere. In this study, we highlight that a persisting high-pressure system over the Europe/Ural region in fall (known as Ural blocking [UB]) can force a delayed response at the surface several weeks later, that resembles the negative phase of the North Atlantic Oscillation (NAO). This is found in two different atmospheric models in which the UB pattern is imposed during the first 2 weeks of November, using a regional relaxation of the troposphere. We also investigate the response to fall/early winter Barents-Kara sea ice decline, which has been hypothesized to have a similar impact on the polar vortex/NAO, but we find that it is of secondary importance compared to the influence of UB.

1. Introduction

Predicting winter weather over populated areas of the Northern Hemisphere (NH) remains a great challenge for climate scientists. Extreme weather events such as the February 2021 Texas cold snap induce catastrophic human and material losses and put great stress on the energy grid (Doss-Gollin et al., 2021). Cold snaps and extreme snowstorms are associated with large perturbations in the mid-latitude flow that induce anomalous persistence of weather patterns in mid-latitudes (e.g., Horton et al., 2015; Pethoukov et al., 2013). Anomalous jet stream configurations that promote extreme weather events are often preceded by anomalies in the polar stratosphere, such as Sudden Stratospheric Warming (SSWs, Butler et al., 2017). While SSWs represent the most extreme state of an anomalous polar vortex in winter, stratospheric vortex displacement events also have impacts at the surface in terms of extreme weather (Kretschmer et al., 2018). Long-range prediction of polar stratospheric variability is therefore of great interest for subseasonal to seasonal (S2S) forecasting and the anticipation of extreme weather events in winter (Domeisen et al., 2020; Vitart & Robertson, 2018).

Many studies have searched for precursors of polar stratospheric warming anomalies, such as blocking patterns in the troposphere (e.g., Bao et al., 2017; Davini et al., 2014; Huang et al., 2017; Kuroda, 2008; Woollings et al., 2010), tropical sea surface temperature (SST) anomalies (e.g., Butler et al., 2014; Fletcher & Kushner, 2011),

snow cover and sea ice concentration (SIC) anomalies (e.g., Cohen et al., 2014; Kim et al., 2014). A key component for intense stratosphere-troposphere interactions seems to be the alignment between anomalous large-scale waves and the background climatological stationary waves. When the two are in phase, they constructively interfere so that upward propagation of planetary waves is amplified, leading to increased wave momentum deposit in the stratosphere and perturbations in the polar vortex (K. L. Smith & Kushner, 2012). For instance, Garfinkel and Hartmann (2008) found that different configurations of the El Niño–Southern Oscillation have different impacts on the polar stratosphere due to differences in how they affect planetary waves and upward wave propagation in the troposphere. Still, it is important to remember that the stratosphere has its own internal variability, such that not all SSWs are preceded by tropospheric wave driving events, and conversely anomalous tropospheric waves are not always followed by an SSW (de la Camara et al., 2019). A better understanding of tropospheric precursors is nevertheless one of the avenues of research for improving S2S forecasts (Karpechko et al., 2018).

Of particular interest is whether anticyclonic anomalies over western Eurasia, also referred to as the Ural blocking (UB) or Scandinavian blocking patterns, can impact the NH winter climate through their influence on the NH polar vortex. These anticyclonic anomalies are part of the mechanism used to explain statistical linkages between the wintertime North Atlantic Oscillation (NAO) and preceding autumn Arctic sea ice and/or Siberian snow cover anomalies (Furtado et al., 2016; Wang et al., 2017). The impact of snow and sea ice anomalies has been questioned due to non-robustness and non-stationarity in the statistical linkages (Kolstad & Screen, 2019; Peings et al., 2013; Siew et al., 2021), and the absence of a robust large-scale atmospheric response in climate sensitivity experiments (Cohen et al., 2020; Henderson et al., 2018; Peings, 2019). In contrast, Peings (2019) showed that a persistent UB pattern induces a robust weakening of the polar vortex and a negative NAO at the surface in the following weeks. Since the UB pattern also induces snow and sea ice anomalies through temperature advection between the high- and mid-latitudes, it is plausible that a significant part of the observed statistical relationships between snow/sea ice and the stratosphere/NAO are an artifact of a common influence exerted by the UB pattern (Tyrlis et al., 2019).

The present study is a follow-up of Peings (2019), hereafter referred to as P19, motivated by different questions. First, what is the response of the polar stratosphere and NAO to more realistic UB anomalies that only persist for 2 weeks (vs. one month in P19)? Second, how do the results compare in two distinct atmospheric models with different spatial resolutions and physics? Third, what is the influence of SIC in the Barents-Kara (BK) Seas on the response to UB? In P19, model experiments with imposed November BK sea ice loss did not produce any significant atmospheric response. However, there is the possibility that BK sea ice anomalies have an indirect influence through the modulation of UB variability, for example, by increasing the persistence of an existing UB pattern. In this paper, we present results from a set of experiments that was designed to answer these questions. We first present the experimental protocol and data we use for this study. The atmospheric response to a persistent UB pattern in early November is described, and compared to the influence of BK sea ice loss, for each model. We then investigate how different BK sea ice conditions modulate the atmospheric response to the UB forcing.

2. Methods

2.1. Numerical Experiments

Two atmospheric general circulation models are used in this study. The Whole Atmosphere Community Climate Model (WACCM) is used with the SC-WACCM4 configuration (CAM4 physics, specified chemistry, K. L. Smith et al., 2014). It has a horizontal resolution of $2.5° \times 1.9°$, 66 vertical levels with a model top at 5.1×10^{-6} hPa (140 km), and a climatological QBO cycle derived from radiosonde data is prescribed. The EC-Earth3 model (Döscher et al., 2021) is used in the Coupled Model Intercomparison Project version 6 (CMIP6) TL255L91 configuration, that is, with $\sim 0.7° \times 0.7°$ horizontal resolution and 91 vertical levels, with last model full-level at 1 Pa. The simulations from the two models are performed with prescribed SST and SIC. In each model control run (CTL), SST/SIC are set to climatological 1979–2008 values from the HadISST data (Rayner et al., 2003), with an AMIP-II correction (AMIP stands for Atmospheric Model Intercomparison Project) to ensure proper monthly means of SST/SIC. External forcings (greenhouse gas, aerosols, solar) are kept fixed to values of year 2000. CTL integrations last 300 yr for WACCM and 50 yr for EC-Earth3.

For each model, two perturbation runs are branched from the control 1 November restarts, each with imposed UB in the first half of November, but different SIC in the BK Seas. The experiments are run from 1 November to

31 January. They include 300 ensemble members for SC-WACCM4 and 50 ensemble members for EC-Earth3. The nudging experiments are designed as follows. From 1 November to 15 November, a blocking anomaly is imposed in a Europe-UB domain (15°W/90°E; 45°N/80°N), from the surface up to 300 hPa. In the literature, the UB is usually defined over a smaller domain that does not include western Europe and/or the east North Atlantic (Davini & D'Andrea, 2020; Yao et al., 2017). For instance, Yao et al. (2017) use the 30°E/90°E longitude band to define UB. However, their Figure 6 shows that the synoptic UB pattern (based on daily data and individual UB events) extends further to the West than the definition implies, at least to 15°W. We found similar results in our own analyses of the UB pattern/index (not shown). For this reason, we nudge the troposphere over a wider domain than the typical UB index domain, so that the full pattern of UB is imposed in the models. For the sake of brevity, the imposed forcing is referred to as the UB pattern in the rest of the study, but it can also be seen as an Ural-European blocking due to its westward spatial extension and the domain of definition. An experiment with reduced westward extension of the nudging domain (starting at 20°E) is discussed in Section 3.1. It shows that the results presented in this study are not sensitive to nudging the troposphere between 15°W and 20°E.

The UB anomaly is imposed by nudging horizontal wind, surface pressure, and temperature in the UB domain toward 3 hr target fields for SC-WACCM4, while vorticity, divergence, temperature, specific humidity, and surface pressure every 6 hr are used for EC-Earth3 target fields (see further details on the nudging protocol for each model in Appendix A). The target fields are constructed by superimposing a UB anomaly on top of the 3-hourly (SC-WACCM4) and 6-hourly (EC-Earth3) fields from the control. Thus, we retain similar high-frequency variability in the perturbation run as in the control, but with a background UB anomaly superimposed in the nudged domain. The nudging linearly decreases between 12 November and 16 November to ensure a smooth transition toward free variability in the model. The UB anomaly is constructed as follows. Daily Z500 anomalies in the UB domain are calculated from the CTL, and we identify UB days (>1 standard deviation of UB index) using a 30-day rolling window for both mean value and standard deviation. A seasonal cycle is then created by compositing fields on the UB days, performing monthly means, and interpolating from 12-month to 3 hr (SC-WACCM4) or 6 hr frequency (EC-Earth3) to create a smooth anomaly file.

Using the UB forcing to constrain the models in the nudging domain, two nudged perturbation experiments are run with different BK sea ice conditions:

- **NUBHI** (November UB High Ice): this experiment has high BK sea ice throughout the run, climatological sea ice everywhere else. The domain for BK sea ice anomalies is 20°E/100°E, 65°N/85°N. The October/November/December (OND) BK SIC field for that run is taken from the year 1988 (HadISST data), the year with highest November and OND SIC in the BK sea over 1979–2021. Prescribing October–December anomalies ensures that the forcing remains consistent throughout November even after daily interpolation of monthly values in the model. Other months have the exact same SST/SIC as the control (1979–2008 climatology with AMIP-II correction).
- **NUBLI** (November UB Low Ice): same as NUBHI, but with low BK sea ice from OND 2016 (lowest on record).

The imposed blocking pattern in both models is shown in Figure 1 with the Z500 anomaly in the first 2 weeks of November, as a result of nudging (as the difference between NUBLI and BKLI, see description below). The Z500 anomalies are about 30% larger in EC-Earth3 compared to SC-WACCM4. Also, we note a fast response to the forcing in EC-Earth3, with an extension of the ridge anomaly over the North Atlantic, although with small amplitude. This is also found in our SC-WACCM experiment with reduced nudging domain (see Section 3.1), so this is not unique to EC-Earth3. Day-by day analyses of the Z500 response show that this signal represents the initial response to the UB pattern outside the forced domain (not shown). It is absent initially but emerges after a few days in the UB experiments.

The daily sea ice anomalies in NUBHI and NUBLI, relative to the control, are shown in Figure 2. Because of the daily interpolation of prescribed monthly means, the anomalies vary smoothly from one mid-month to the next. The 1988 high BK sea ice forcing represents about +1.5 standard deviation anomaly, relative to the 1979–2021 climatology. The 2016 low BK sea ice forcing represents about −3 standard deviation anomaly. The amplitude of the SIC forcing peaks in mid-November and it stays relatively high until mid-December (0.3–0.4 fraction anomaly) until it linearly decreases to 0 in mid-January. The spatial pattern of SIC anomalies is visible in Figure S1 in Supporting Information S1, along with associated changes in the 2 m temperature. These experiments allow us to

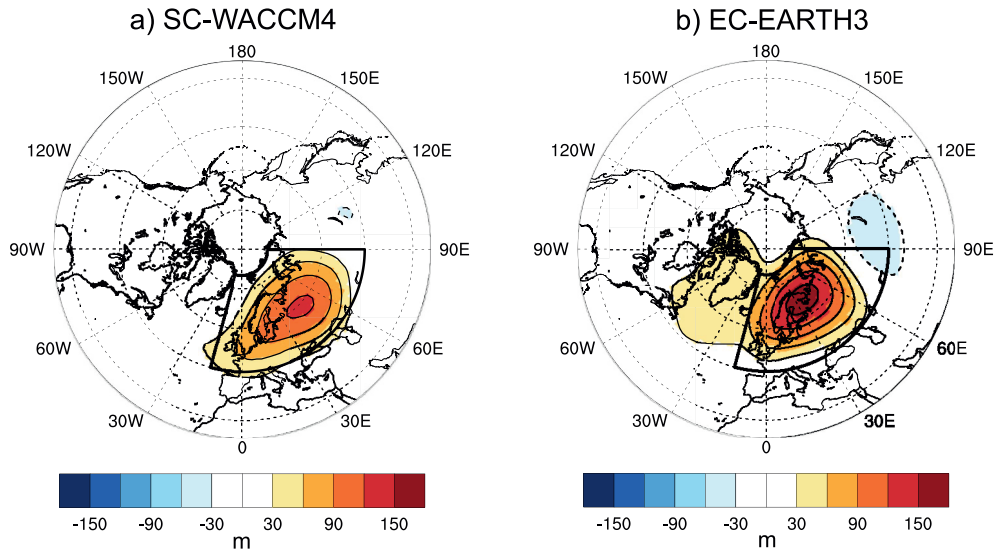

Figure 1. Z500 anomalies (contour interval 30 m) during the first 2 weeks of November when Ural blocking (UB) is imposed in the models through nudging of the troposphere in the 45°/80°N, 15°W/90°E domain (see black box): (a) for the SC-WACCM4 experiments (UBLI shown here); (b) same as (a) for EC-Earth3.

explore whether different sea ice conditions in the BK seas have an influence on the persistence of the UB pattern (once the nudging is turned off), and on the following atmospheric response to the UB anomaly.

The SST is also changed in the BK domain, only where SIC changes by more than 0.1 (unit: fraction of SIC). Linear smoothing is applied at the edges of the domain to ensure smooth transition from the high/low ice field to the 1979–2008 climatology used in the control.

Two additional simulations with only sea ice anomalies in the BK Seas have been performed. They also include 300 ensemble members for SC-WACCM4, but this time 100 ensemble members for EC-Earth. Additional ensemble members for EC-Earth3 are branched from 1 November initial conditions that have been produced by randomly perturbing 1 October CTL integrations. They include no UB anomaly, hence they isolate the impact of BK SIC, that we can compare to the impact of the UB forcing.

- **BKHI** (BK High Ice): similar to NUBHI, but without the nudged UB anomaly
- **BKLI** (BK Low Ice): similar to NUBLI, but without the nudged UB anomaly

The response to UB under low BK SIC is represented by the difference in ensemble means of NUBLI and BKLI. The NUBLI minus BKLI difference is referred to as the UBLI response in the paper. Similarly, the response to

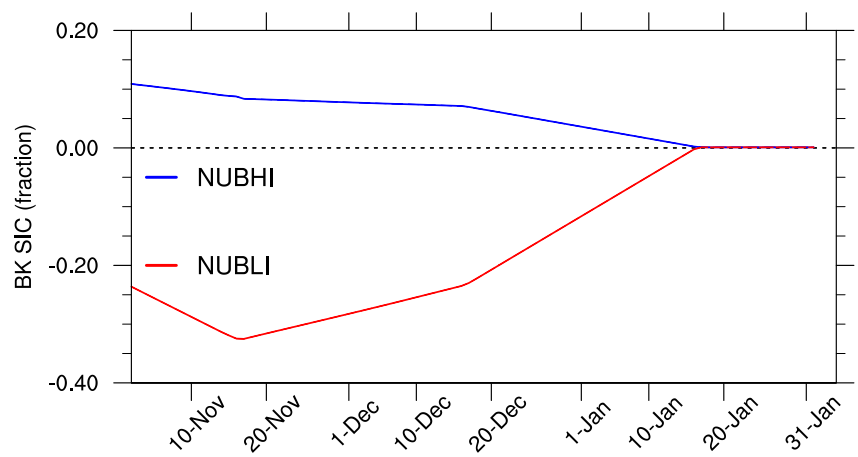

Figure 2. Daily Barents-Kara (BK) sea ice concentration (SIC) anomalies (fraction) in SC-WACCM4 and EC-Earth3 experiments NUBHI (blue) and NUBLI (red), relative to the control run.

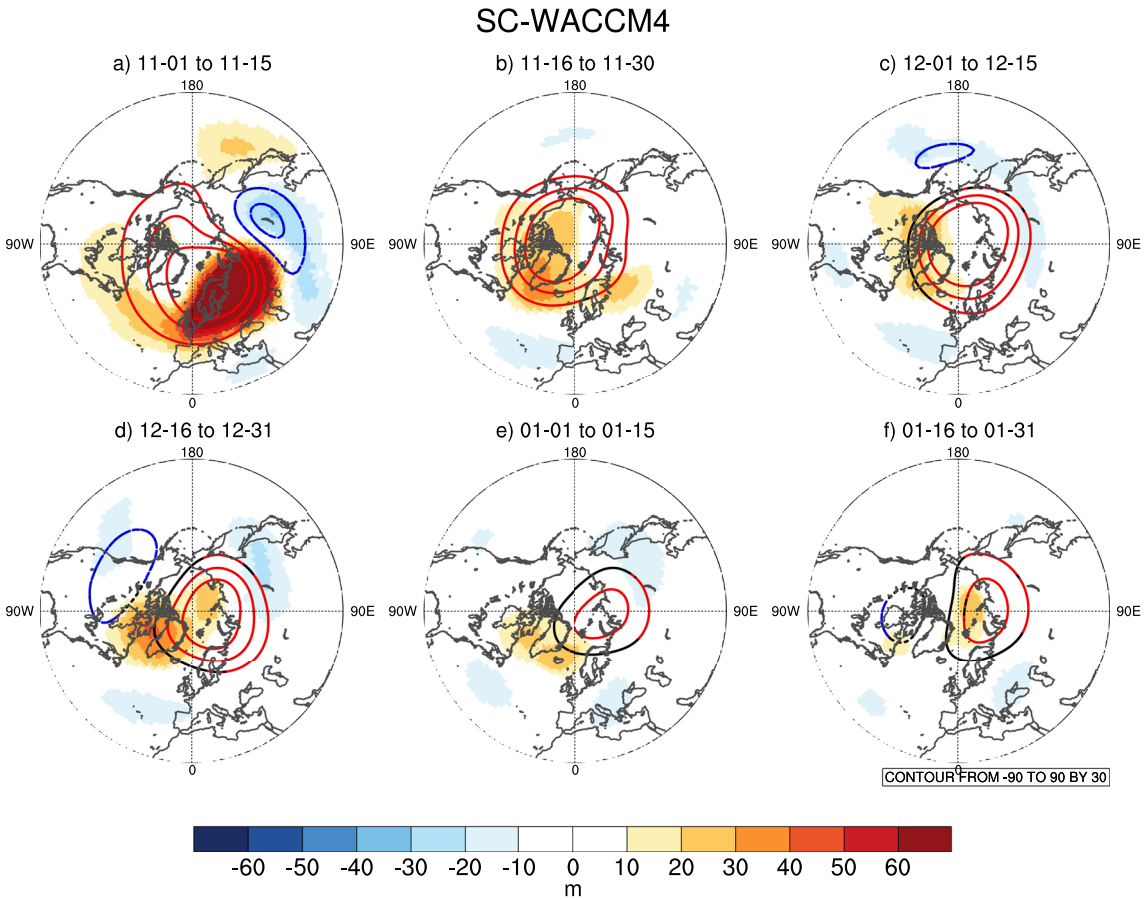

Figure 3. Anomalies of Z500 (shading, 10 m contour interval) and Z50 (contours, 30 m contour interval) in SC-WACCM4 experiments NUBLI minus BKLI (impact of Ural blocking [UB] under low Barents-Kara [BK] sea ice), averaged over: (a) 1–15 November; (b) 16–30 November; (c) 1–15 December; (d) 16–31 December; (e) 1–15 January; (f) 16–31 January. Only Z500 anomalies that are significant at the 95% confidence level are shown. Red/Blue Z50 contours represent anomalies that are significant at the 95% confidence level.

UB under high BK SIC, represented by the NUBHI minus BKHI difference, is referred to as UBHI. The response to sea ice loss is referred to as BKLI.

2.2. Statistical Significance

The statistical significance of the results is verified using a two-tailed Student *t* test, the null hypothesis being that the difference between two experiments only happens by chance. We use a threshold *p* value of 0.05 to reject this null hypothesis with a confidence level of 95%. A more stringent method that tests reproducibility and consistency of the results has been tested (Peings et al., 2021). However, we found that the main signals identified in this paper are robust and generally consistent in 50 yr subsets of the experiments, as discussed in the results section, so the Student *t* test is sufficient to identify the robust signals in this study.

3. Results

3.1. Large-Scale Atmospheric Response to the UB Anomaly

The response to the UB forcing under low sea ice conditions (UBLI) in SC-WACCM4 is shown in Figure 3. Each panel corresponds to biweekly averages of geopotential height at 500 hPa (Z500) and at 50 hPa (Z50), from 1–15 November to 16–31 January. Figure 4a complements this view by showing the detailed timing of the polar cap response using daily data. The upper panels of Figure 4 represent the response of the geopotential polar cap (north of 65°N, referred to as Zcap) as a function of time and pressure levels, along with the anomaly in upward

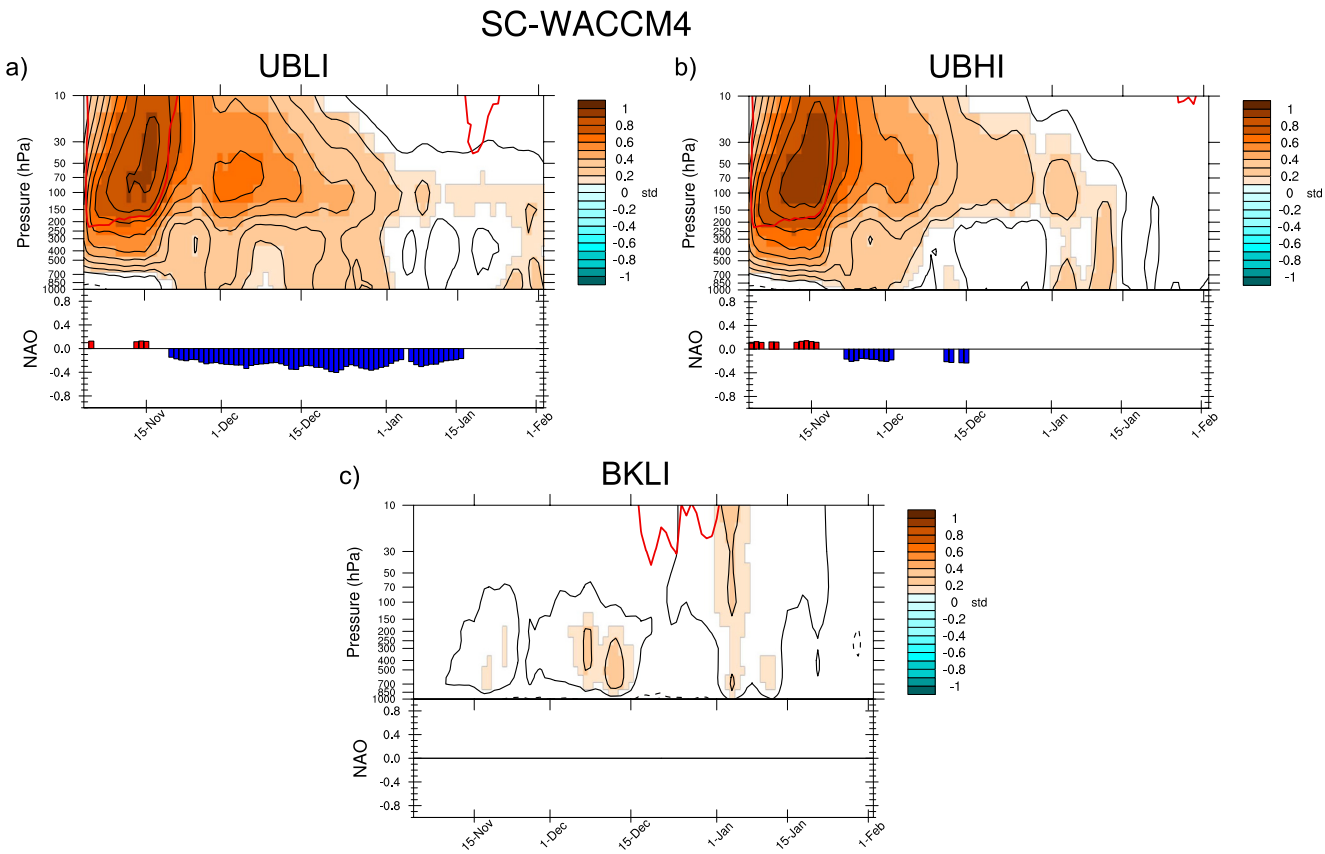

Figure 4. (a) Daily anomalies of normalized polar cap geopotential height (averaged north of 65°N), in function of time and height (black contours, 0.1 standard deviation interval), in SC-WACCM4 experiments NUBLI minus BKLI (impact of Ural blocking [UB] under low Barents-Kara (BK) sea ice). Shading indicates anomalies that are significant at the 95% confidence level. The red contours show upward WAFz pulses in the stratosphere (zonal average between 40°N and 80°N) that are significant at the 95% confidence level (1 standard deviation contour). The bottom panel shows the corresponding daily North Atlantic Oscillation (NAO) anomalies, only shown when they are significant at the 90% confidence level. (b) Same as (a) but for the response in SC-WACCM4 experiments NUBHI minus BKHI (impact of UB under high BK sea ice). (c) Same as (a) but for the response in SC-WACCM4 experiments BKLI minus BKHI (impact of BK sea ice loss).

planetary wave activity (Plumb flux, WAFz) entering the polar stratosphere. The lower portion of the panels show the response of the daily NAO index, red (blue) bars indicating a positive (negative) NAO anomaly.

In 1–15 November (Figure 3a), we see the imposed UB forcing with a large anticyclonic anomaly over the Ural domain. It is accompanied by lower Z500 over Siberia, resulting in a ridge-trough pattern over Eurasia that promotes upward wave activity flux over this region (the response of the 150 hPa vertical Plumb flux component is shown in Figure S2 in Supporting Information S1). The polar stratosphere warms over the UB sector and in the entire Arctic region, showing increased geopotential height (Z50 contours), but unlike the UB signal, it persists after the nudging is turned off (Figures 3b–3f). The polar vortex remains significantly warmer (i.e., weaker) until January, and this is associated with a dipole of Z500 anomalies that resembles the negative phase of the NAO, with anticyclonic anomalies in the subpolar Atlantic, and cyclonic anomalies in the mid-latitudes (Figures 3b–3e). This is also visible in Figure 4a. As anomalously high upward wave activity enters the polar stratosphere during the first half of November (red contour), Zcap anomalies are positive throughout the atmospheric column. The associated weakening of the polar vortex persists until the end of December, and consistent with top-down influence of the polar stratosphere it is associated with a negative NAO index at the surface. In January, the polar vortex response diminishes, and at the end of the month scant significant Z500 anomalies remain (Figure 3f). These results support the findings from P2019, although the response is weaker here due to a less persistent and less intense UB forcing. Figure 4b shows the same anomalies but for UBHI. Despite a mostly similar response of the polar stratosphere and wave activity flux in November, the polar vortex weakening is not as pronounced in December, and negative NAO anomalies persist less than in UBLI. We will come back to this in Section 3.3.

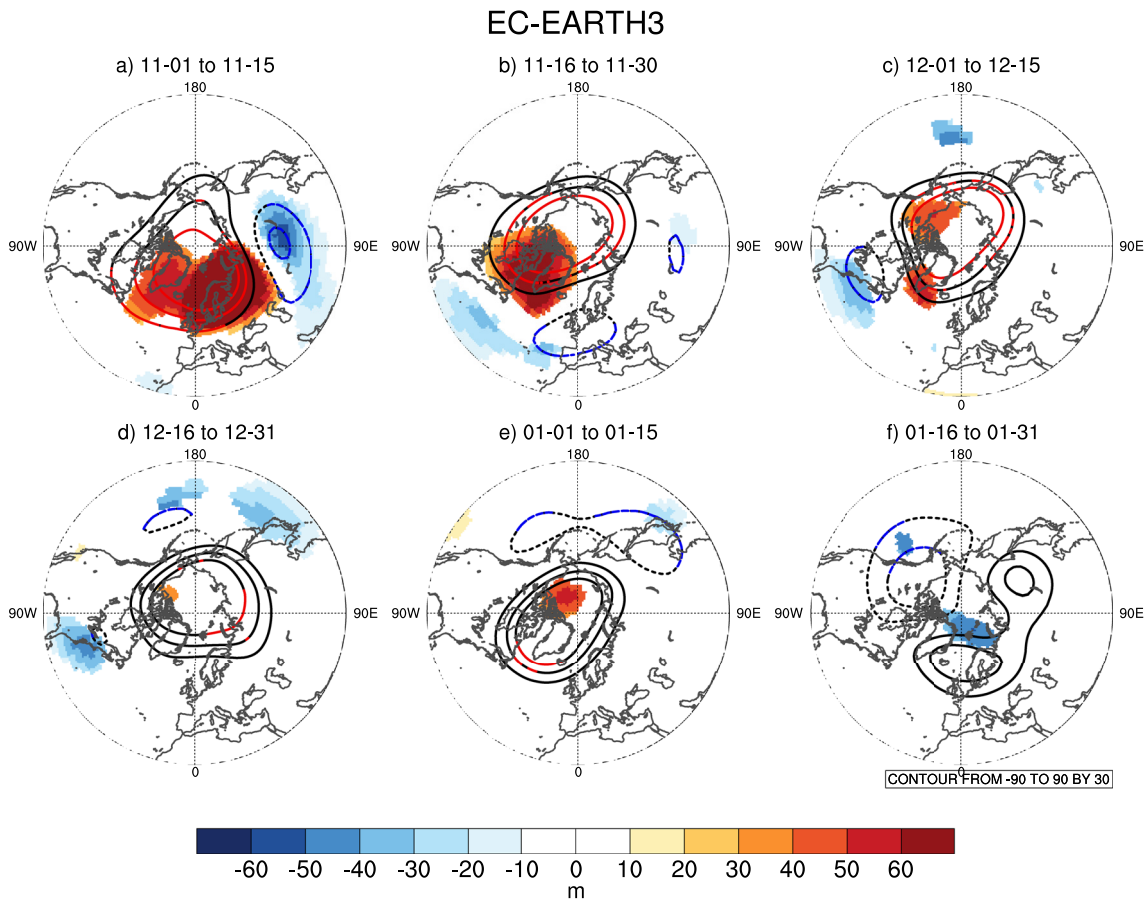

Figure 5. Same as Figure 3 but for EC-Earth3.

Figures 5 and 6 are equivalent to Figures 3 and 4, but for EC-Earth3. The overall response is very consistent with the results from SC-WACCM4. Note that the anomalies are less statistically significant, despite larger amplitude in the troposphere, but this is expected from the smaller ensemble size in the EC-Earth3 simulations. Similar to SC-WACCM4, the polar vortex warms in response to the UB anomaly, and stays anomalously warm until mid-January (Figures 5 and 6a). A negative NAO pattern is found in the troposphere from early November to mid-December, that is, 1 month after the UB anomaly is released. The response of Zcap is also very consistent with SC-WACCM4, with positive height anomalies that persist until mid-January in the lower stratosphere, and episodes of downward propagation toward the surface that are associated with the negative NAO (Figure 6a). The negative NAO anomalies persist less than in SC-WACCM4, but remember that the latter has a larger sample size that allows for smoother signals. To illustrate the role of ensemble size, Figure S3 in Supporting Information S1 shows the Z500 and Z50 monthly anomalies in the six 50-member subsets of the full ensemble of SC-WACCM4 runs. Although a weakening of the polar vortex is found in each subset, its amplitude varies so that the associated NAO response in the troposphere is not always similar. Therefore, we cannot conclude that the weaker NAO response in EC-Earth3 is due to differences in structural model differences, since it is consistent with fluctuations that can be expected from internal variability alone. Coming back to EC-Earth3, the polar stratosphere warming is associated with increased wave activity flux throughout November and early December (red contours in Figure 6a). Again, results are noisier than in the SC-WACCM4 experiments due to smaller ensemble size, but they are remarkably consistent. In EC-Earth3 too, UBHI exhibits less persistence in the negative NAO response, consistent with reduced persistence in the polar vortex warm anomalies (Figure 6b).

The sensitivity to the westward extent of the nudging domain has been tested in SC-WACCM4, with an experiment similar to NUBLI (300 ensemble members too), but with nudging only applied between 20°E and 90°E, instead of 15°W/90°E (same latitudinal extent 45°N/80°N). The corresponding UB forcing imposed in this experiment is shown in Figure 7a. Despite the reduced domain, positive Z500 anomalies propagate rapidly over

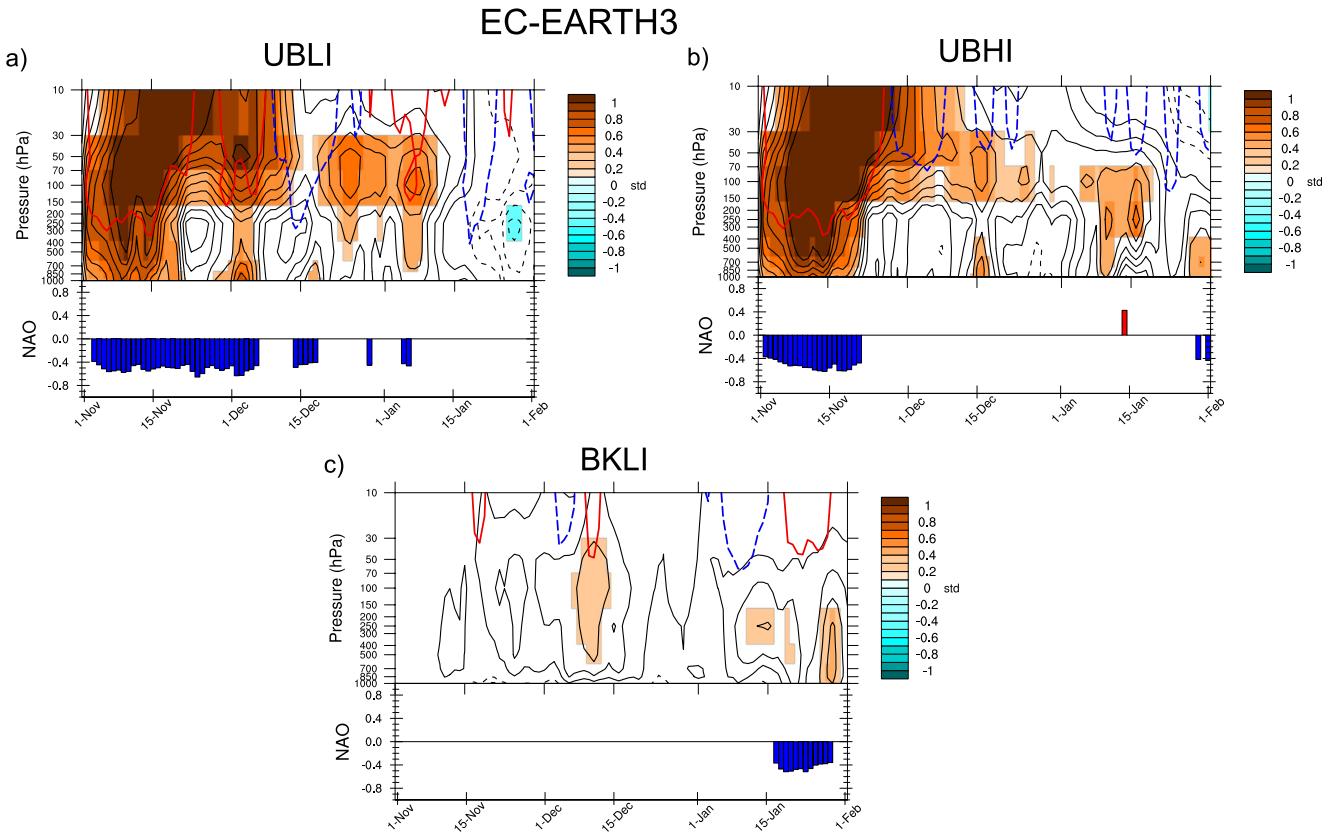

Figure 6. Same as Figure 4 but for EC-Earth3.

the North Atlantic in the first 2 weeks (Figure 7a), and the delayed response of the polar vortex and NAO is very similar to the response we obtain with the original UB domain (Figure 7b). We conclude that the results are not very sensitive to the westward extension of the nudging UB domain, and that the polar vortex/NAO response is mostly a response to ridging over the Eastern/Europe-Ural sector of the nudging domain.

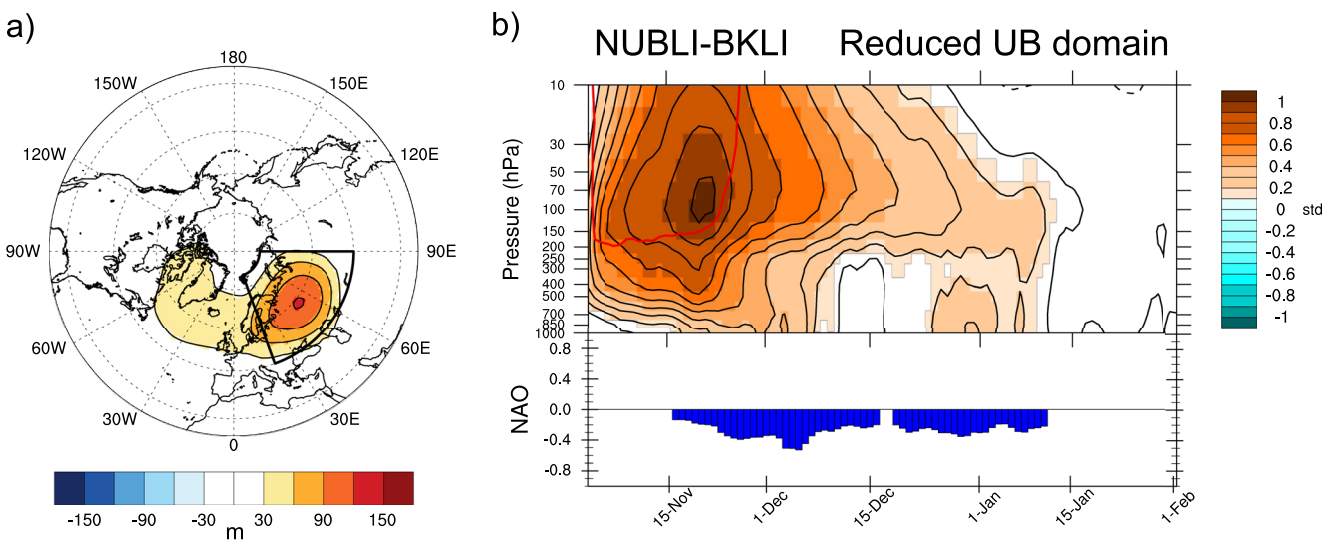

Figure 7. Results from an experiment with reduced Ural blocking (UB) nudging domain. (a) Z500 anomalies (contour interval 30 m) during the first 2 weeks of November. The nudging domain starts at 20°E, rather than 15°W in the original experiment; (b) same as Figure 4a but using the NUBLI experiment with reduced domain. Results are very similar, suggesting low sensitivity to the westward extent of the blocking anomaly.

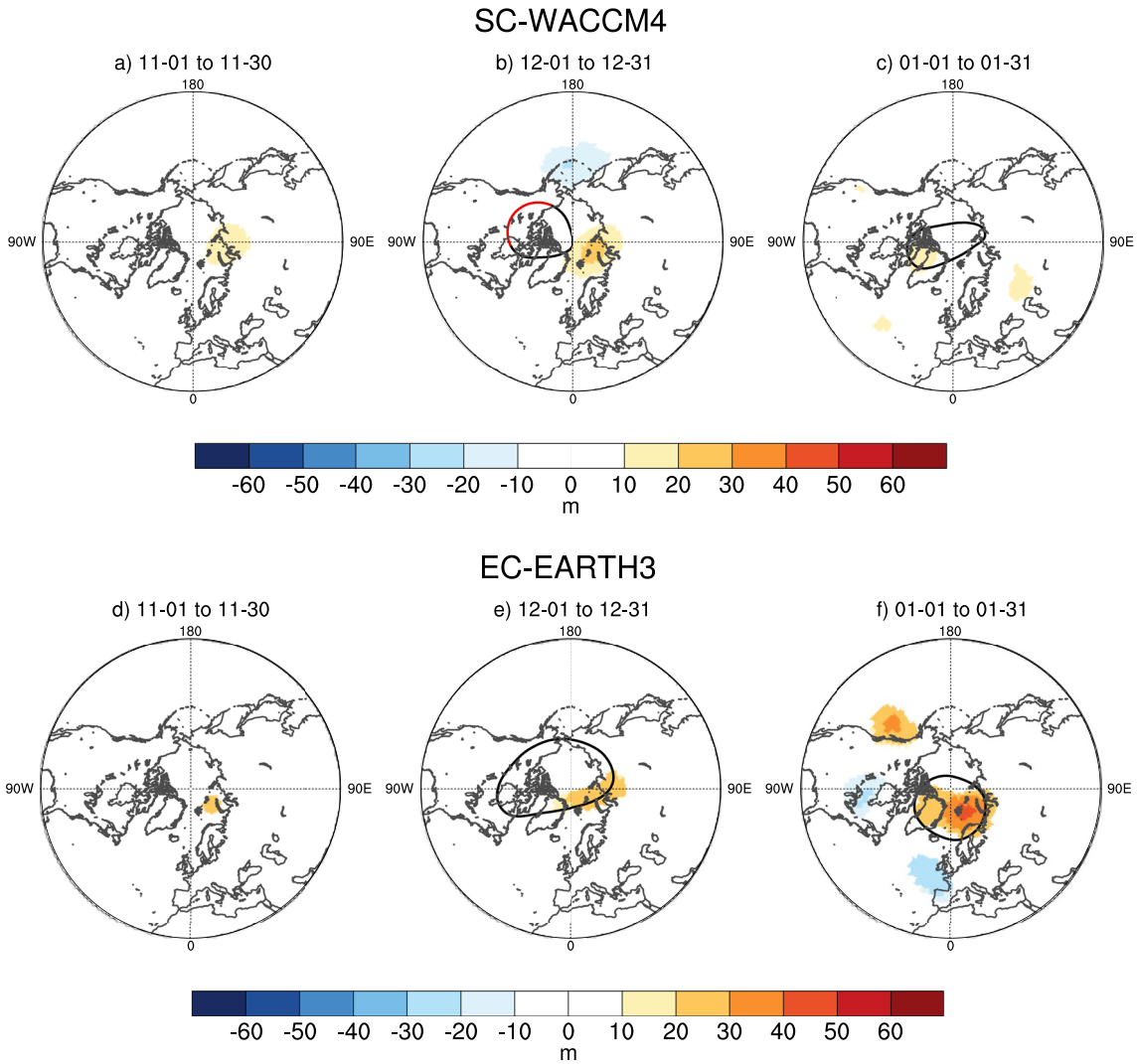

Figure 8. Anomalies of Z500 (shading, 10 m contour interval) and Z50 (contours, 30 m contour interval) in SC-WACCM4 experiments BKLI minus BKHI (impact of BK sea ice loss), in: (a) November; (b) December; (c) January. (d–f) Same as (a–c) but for EC-Earth3. Only Z500 anomalies that are significant at the 95% confidence level are shown. Red/Blue Z50 contours represent anomalies that are significant at the 95% confidence level.

3.2. Impact of BK Sea Ice Loss

Comparing the BKHI and BKLI experiments of each model, we can isolate the response to BK sea ice loss alone (BKLI). In Figure 8, we show monthly averages of the Z500 and Z50 responses in each model. A more detailed timing of the response is shown in Figures 4c and 6c (daily Zcap and NAO anomalies), as well as in Figures S4 and S5 in Supporting Information S1 that show 2-week averages of the Z500/Z50 anomalies. Despite the fact that the sea ice anomalies persist longer than the UB forcing (remember sea ice loss is imposed from November until mid-January), no strong large-scale atmospheric response is found in these experiments (Figure 8). In SC-WACCM4, a moderate amplitude Z500 ridge anomaly is found above the BK seas from mid-November to mid-December (Figures S3b–S3c in Supporting Information S1), and a small warming of the polar stratosphere occurs from mid-December to mid-January in association with moderate anomalous upward wave activity entering the polar stratosphere (Figure 4c). However, this warming of the polar stratosphere is hardly statistically significant (Figures S4d–S4e in Supporting Information S1), and it does not induce any NAO response (Figure 4c).

EC-Earth3 exhibits a weak negative NAO response in January, with a ridge over the BK Seas, and weak low-pressure anomalies in the mid-North Atlantic (Figure 8f). In fact, the BK Seas ridge is also found in the first half of December, but disappears in the second half, so that the December monthly mean does not show a significant signal (Figure S5 in Supporting Information S1). The negative NAO response found at the end of

January is also visible in Figure 6c. Interestingly, it is not associated with any significant signal in the polar stratosphere, suggesting it is a purely tropospheric response. Except for this negative NAO signal at the end of January, EC-Earth3 does not respond strongly to BK sea ice loss. The weak sensitivity to BK sea ice loss in the two models is consistent with P19 that found almost no response to November BK sea ice loss. In the current experiments, and despite the fact that unlike P19, we maintain sea ice loss throughout December and early January, similar conclusions are reached. When forced with present-day BK sea ice loss, our two models fail to reproduce a strong large-scale atmospheric response, in particular, a significant polar vortex perturbation and a cooling over Siberia.

The response of the 2 m temperature (T2M) to BK sea ice loss and the UB is shown in Figure 9, along with the sea-level pressure (SLP) response, for both models. In SC-WACCM4, the only significant SLP response to sea ice (BKLI) is a low-pressure anomaly directly above sea ice loss, in the maximum of T2M warm anomaly (Figures 9a–9c). No cooling is found over Siberia. In contrast, the UB anomaly induces a dipole of T2M anomaly that resembles the Warm Arctic Cold Siberia (WACS) pattern (Figure 9d). After the forcing is removed, only the cold anomaly persists over Siberia (Figures 9e and 9f). It is driven by a high-pressure anomaly at higher latitudes that is consistent with the positive node of the negative NAO/Northern Annular Mode (NAM, Thompson & Wallace, 2000). In other words, the direct effect of UB is to drive the WACS pattern, and its delayed impact in terms of surface temperature over Eurasia is consistent with the negative NAO. The T2M/SLP response is broadly similar in EC-Earth3 (Figures 9g–9l). The nudging results in stronger positive SLP anomalies in the UB region and beyond than in SC-WACCM4, inducing a stronger cooling over Siberia in November (Figure 9j). However, in December and January, the positive SLP anomalies over Siberia are less pronounced than in SC-WACCM4, and the associated cooling is mostly absent. Interestingly, the negative NAO pattern in December is more pronounced than in SC-WACCM4, and it looks like the negative NAM since low-pressure anomalies are also found over the North Pacific. In summary, despite differences in the surface temperature anomalies, the simulations from the two models agree on the sign of the NAO/NAM response at the surface and on the central role of UB in driving the WACS response.

3.3. Does BK Sea Ice Modulate the UB Teleconnection?

Although BK Sea ice loss does not exert a strong influence on the large-scale atmospheric response in our experiments, it seems to modulate the response to the UB anomaly (Figures 4 and 6). This can happen either by increasing persistence in the UB forcing, or by providing different background climate conditions. The latter possibility can be explored by comparing the UBLI response with the UBHI response. But first, we want to verify whether BK sea ice impacts the persistence of the UB pattern, after nudging is turned off.

Figure 10 shows the daily evolution of the UB Z500 anomaly in NUBHI and NUBLI, relative to the CTL, in the two models. By design, over 1–15 November a positive anomaly is found that corresponds to imposing the UB pattern through nudging. After 15 November, the UB area is not nudged anymore and we can verify whether the different BK sea ice conditions affect the persistence of the UB anomaly. In SC-WACCM4, the Z500 UB anomaly does not persist longer in NUBLI. It quickly converges toward 0, although it remains slightly higher in December and January in NUBLI. However, the NUBLI versus NUBHI difference is very small relative to internal variability (represented by the ± 2 standard deviation envelope). EC-Earth3 exhibits larger differences between the two runs. In NUBLI, the Z500 UB index persists longer in November and early December, in comparison with NUBHI (Figure 10b). It remains slightly higher in NUBLI in December and early January, but again, the signal is small, and because the EC-Earth3 experiments only include 50 ensemble members, the influence of internal variability is surely larger than in SC-WACCM4.

Even though BK sea ice does not appear to significantly influence the persistence of the UB pattern, the reduced persistence of negative NAO anomalies in UBLI (Figures 4b and 6b) suggests that BK SIC modulates the UB teleconnection. This is further explored by comparing the UBLI and UBHI responses. Figures 11a–11d show latitude versus time plots that represent the tropospheric response in the North Atlantic [60°W/60°E sector] in SC-WACCM4, through U700 anomalies (shading) and transient eddy activity (red contours). The transient eddy activity is defined as the standard deviation of 2–8 days bandpass filtered Z500 daily anomalies, the standard deviation being calculated over an 11-day moving window. It is used as a proxy for the storm track. We are interested in the response of the transient activity since eddy-mean flow interactions may play a role in the persistence of the negative-NAO response. Panels 11e–11h show the corresponding response of the polar stratosphere, using a similar latitude versus time plot, but for Z50 anomalies. To further complement this view, the UBLI minus UBHI difference in biweekly anomalies of T2M and Z50 is shown in Figure 12 for SC-WACCM4. Equivalent figures to Figures 11 and 12, but for EC-Earth3, are shown in SI (Figures S6 and S7 in Supporting Information S1). The

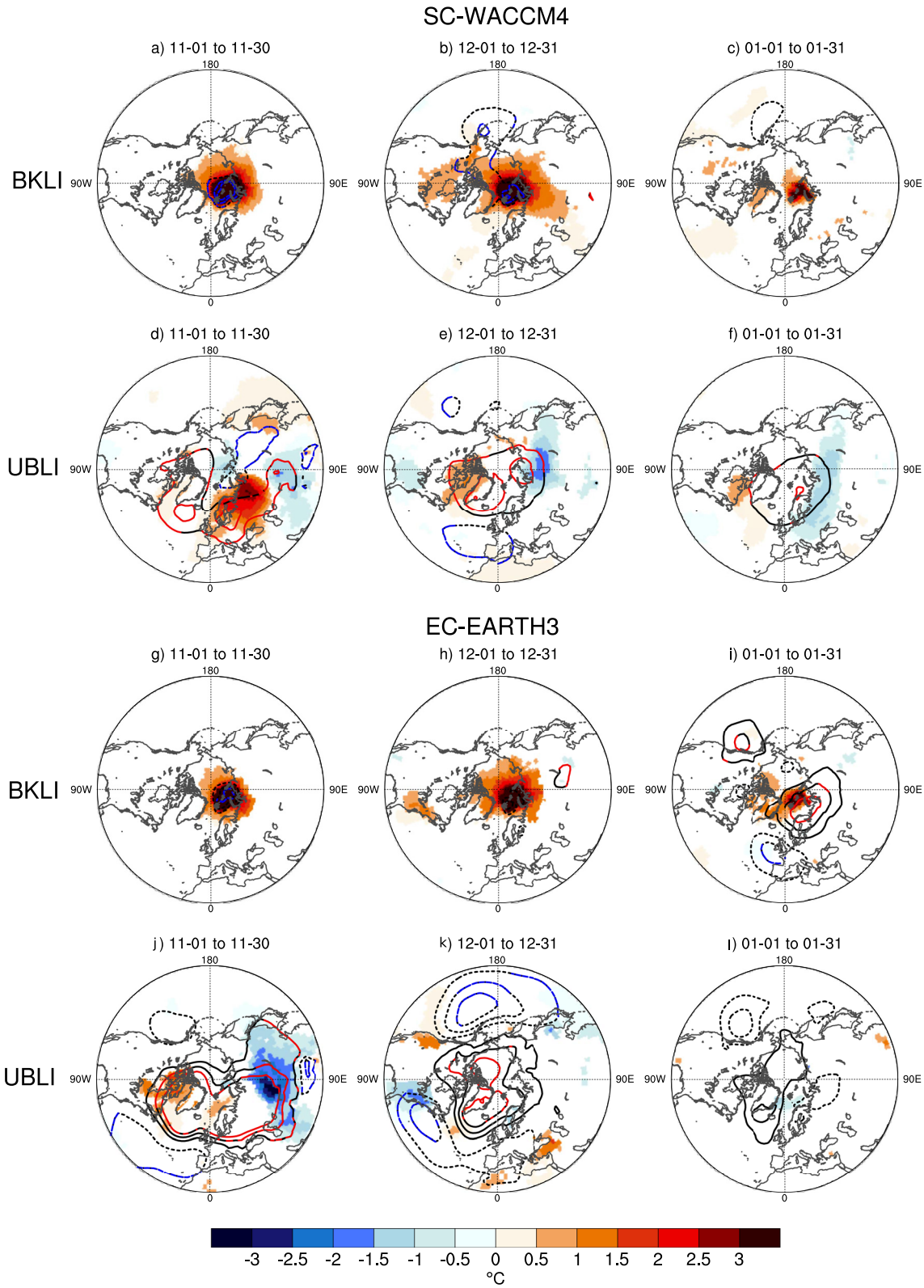

Figure 9. Anomalies of T2M (shading, 0.5°C contour interval) and sea-level pressure (SLP) (contours, 1 hPa contour interval) in SC-WACCM4 experiments BKLI minus BKHI (impact of BK sea ice loss), averaged over: (a) November; (b) December; (c) January. (d–f) Same as (a–c) but for the SC-WACCM4 experiments NUBLI minus BKLI (impact of UB under low BK sea ice). (g–l) Same as (a–f) but for EC-Earth3. Only T2M anomalies that are significant at the 95% confidence level are shown. Red/Blue SLP contours represent anomalies that are significant at the 95% confidence level.

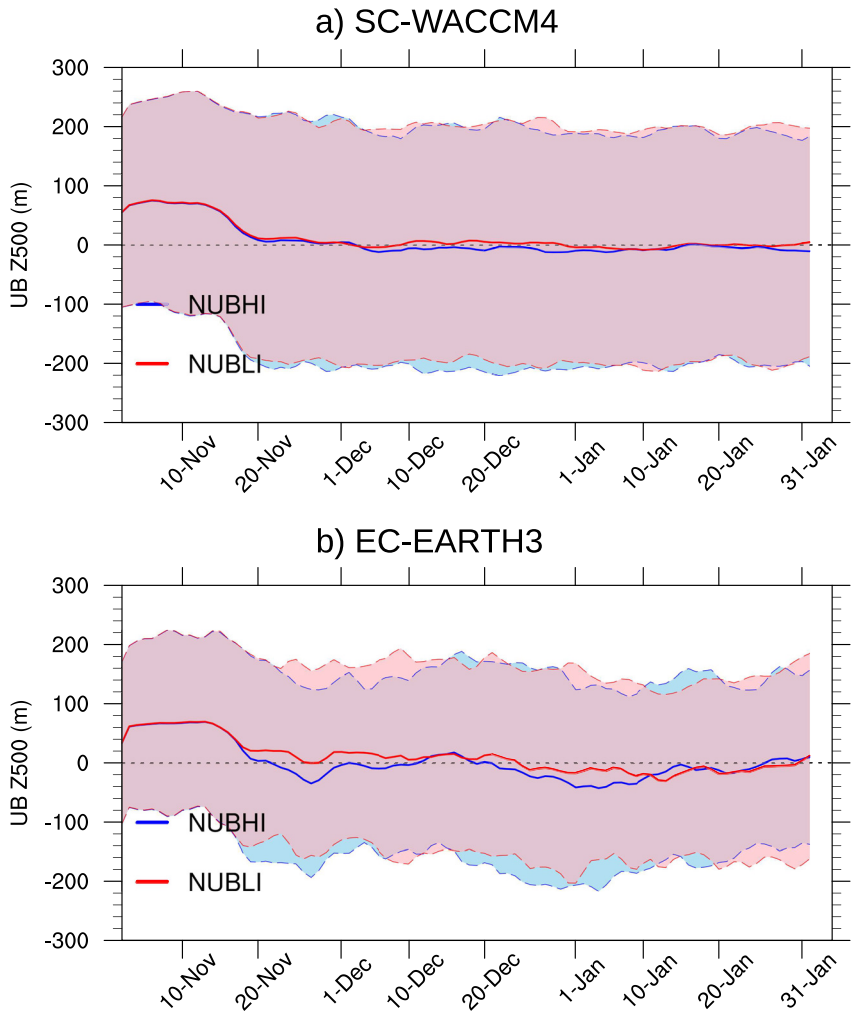

Figure 10. Daily anomaly of Z500 (m) in the Ural blocking domain (nudged domain), for NUBHI (blue) and NUBLI (red), in: (a) SC-WACCM4; (b) EC-Earth3. The envelope shows ±2 standard deviations from the ensemble spread (300 ensemble members for SC-WACCM4, 50 for EC-Earth3).

smaller sample size in EC-Earth3 makes it more difficult to compare the difference in responses between two pairs of experiments, so we mostly focus on SC-WACCM4 in this section.

In both UBLI and UBHI, the imposed UB anomaly induces a deceleration and then an equatorward shift of the North Atlantic westerly flow (Figures 11a and 11b). The deceleration is almost instantaneously associated with a weaker polar vortex (Figures 11e and 11f). The decrease in westerly flow is associated with reduced transient activity, as expected from eddy-mean flow feedbacks (Figure 11, red contours), consistent with a negative NAO as shown earlier. In comparison, the impact of BK SIC alone, both in the troposphere and stratosphere, is remarkably weaker (Figures 11d and 11h). In line with results from Section 3.1, we find that the UBLI response persists longer than UBHI (Figure 11a vs. Figure 11b). This is especially true in December and January, as illustrated in Figure 11c where the difference between the two responses is shown. The equatorward shift/deceleration of the westerly flow is greater in UBLI, as is the reduction in storm track activity. The comparison between Figures 11c and 11d illustrates that although BK SIC loss alone does not drive a significant response over the North Atlantic, when a UB anomaly is imposed, BK SIC conditions make a difference in the atmospheric sensitivity to the forcing (i.e., there are nonlinear interactions at play).

A plausible mechanism to explain the greater response in UBLI is the response of the polar stratosphere, which warms more, compared to UBHI, in December and January (Figures 11g and 12c–12d). This likely promotes larger NAO response at the surface. Nonlinear effects are clearly at work here, since no response of the polar vortex is found in

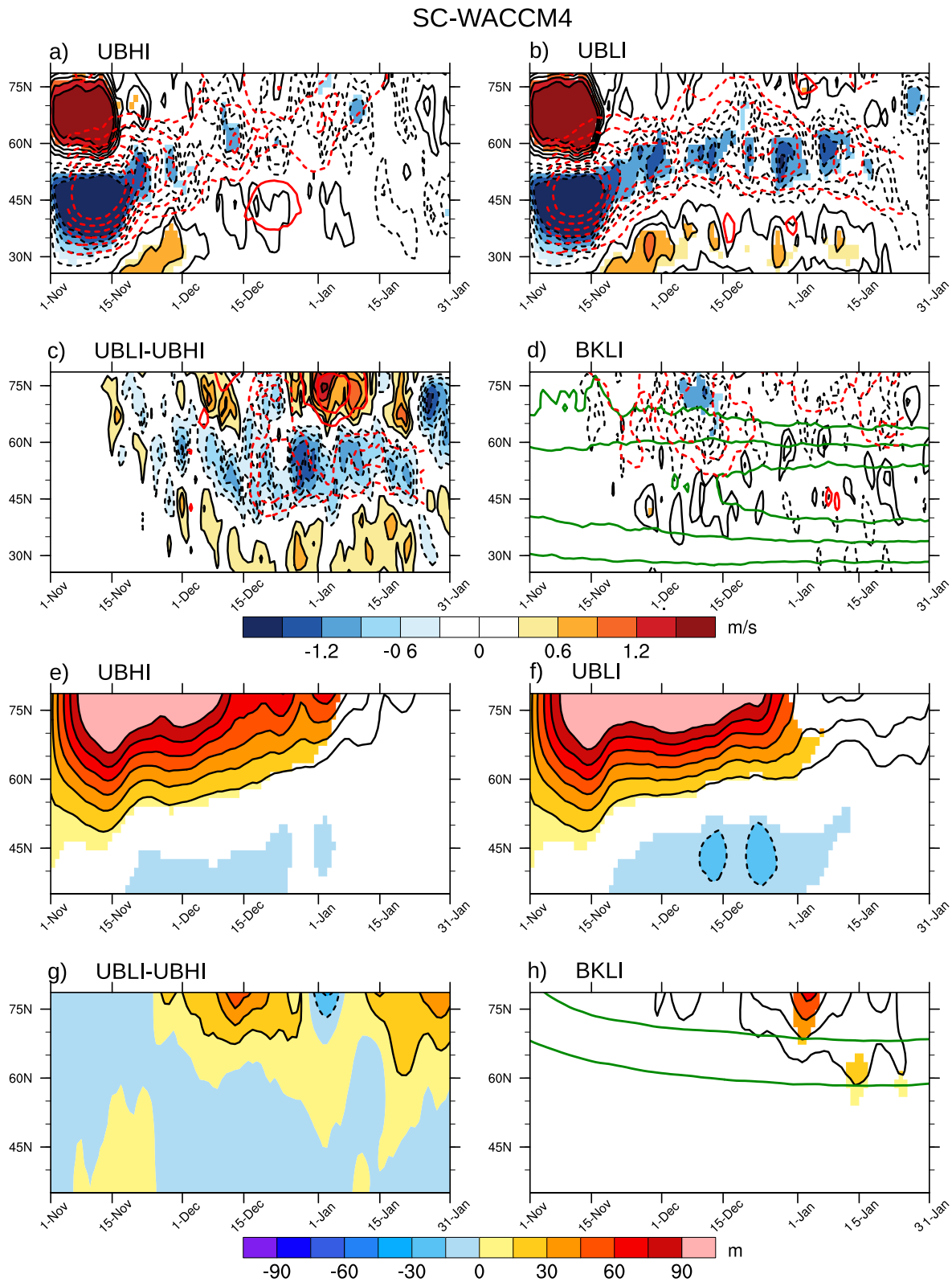

Figure 11.

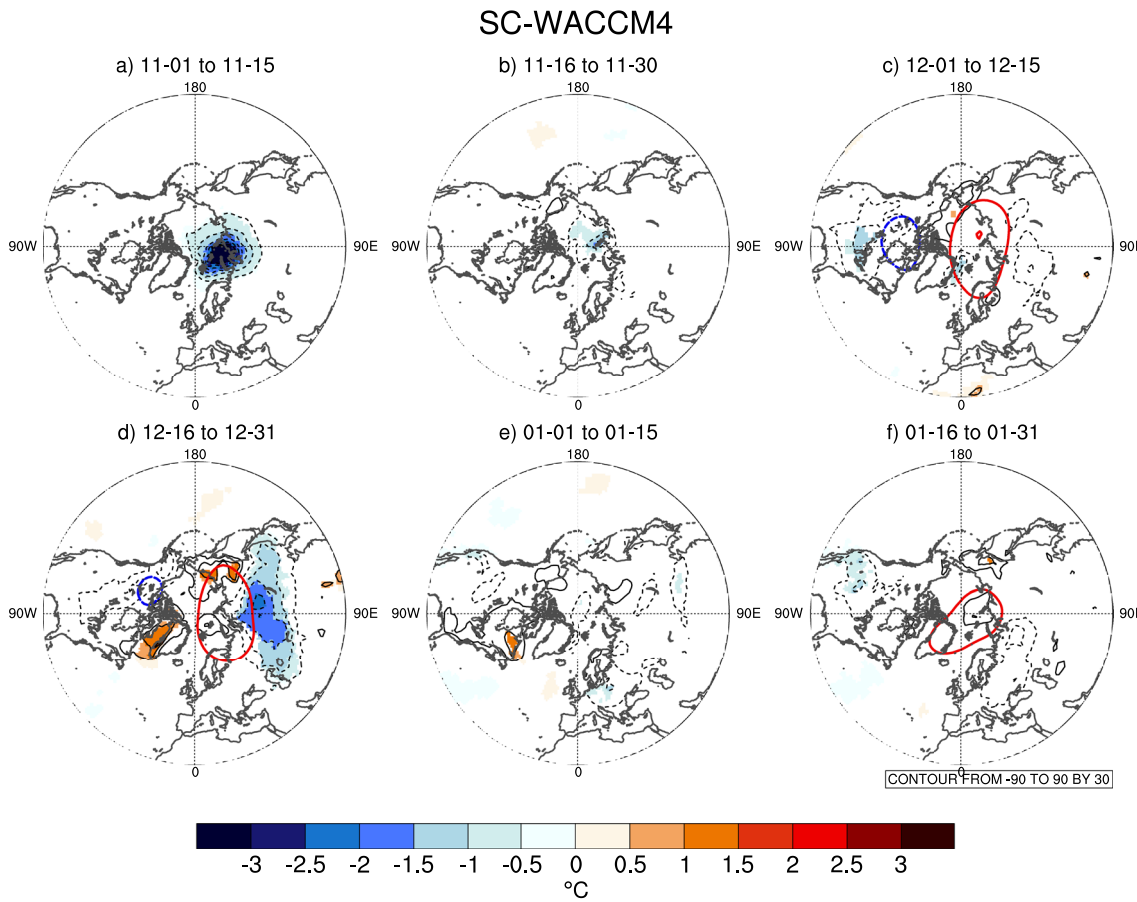

Figure 12. Difference in the T2M (shading/black contours, 0.5°C contour interval) and Z50 (contours, 30 m contour interval) response to the Ural blocking (UB) anomaly in SC-WACCM4, depending on the Barents-Kara (BK) sea ice conditions, that is, difference between the NUBLI-BKLI and the NUBHI-BKHI responses. (a) 1–15 November; (b) 16–30 November; (c) 1–15 December; (d) 16–31 December; (e) 1–15 January; (f) 16–31 January. Only T2M anomalies that are significant at the 95% confidence level are shown.

December in BKLI (Figure 11h). A similar result is found in EC-Earth3, although with a different timing (Figure S6 in Supporting Information S1). The polar vortex warming is larger in UBLI in December and early January (Figure S6g in Supporting Information S1), when the decrease in westerly flow is more pronounced (Figure S6c in Supporting Information S1). The difference in polar vortex response in EC-Earth3 UBLI versus UBHI is difficult to interpret though, as it looks quite noisy from one biweekly average to the other (Figure S7 in Supporting Information S1).

An interesting finding is that in early November, the BK T2M response to UB is about three times larger in UBHI than in UBLI. This is seen as a negative T2M anomaly in Figure 12a. This result can be understood by the fact that in UBLI, the temperature is already anomalously warm in the BK region (compared to CTL, not shown), and the advection of midlatitude warm air by the UB has less impact than in UBHI, when the region is anomalously cold. In other words, sea ice conditions modulate nonlinearly the magnitude of the warming induced by UB in the BK region. This effect is also found in EC-Earth3 (Figure S7a in Supporting Information S1).

However, it is unclear if this different sensitivity of concomitant BK T2M to UB plays a role in the larger polar vortex warming found in December. Indeed, our analyses have not allowed us to pinpoint the origin of the enhanced persistence of the polar vortex response in UBLI, also due to the small signal-to-noise ratio. The

Figure 11. SC-WACCM4 - North Atlantic sector [60°W/60°E] - latitude versus time plot of U700 anomalies (shading/black contours, 15 m/s contour interval) and transient eddy activity (storm track, red contours, 1m contour interval), in response to: (a) Ural blocking (UB) under high Barents-Kara (BK) sea ice concentration (SIC); (b) UB under low BK SIC; (c) UBLI minus UBHI; (d) BK sea ice loss. Shading indicates U700 anomalies that are significant at the 95% confidence level, except in (c) where no statistical test is applied. Transient activity is defined as the 11-day moving-window standard deviation of Z500, bandpass filtered to only retain 2–8 days variability (unit, m). The green contours in (d) show the climatology of U700 (contour interval, 3 m/s). (e–h) Same as (a–d) but for Z50 anomalies (m), over all longitudes [0°/359°E].

possible role of snow cover, which might provide memory for the BK T2M anomaly throughout winter, was assessed without finding any significant linkage. We can only conclude the polar vortex recovers more slowly from the wave forcing imposed by UB in early November in UBLI. How that is exactly happening will need to be determined in future work, especially with different models/protocols to ensure the robustness of this finding.

In summary, the two models suggest that although BK sea ice anomalies alone cannot drive significant UB anomalies and the associated polar stratosphere/NAO response (except at the end of January in EC-Earth3), they can modulate how the polar stratosphere/NAO respond to a persistent UB pattern in early November. Sea ice loss makes the atmosphere more sensitive to UB anomalies in both models.

4. Conclusion

This paper analyzes perturbation experiments from two atmospheric models, SC-WACCM4 and EC-Earth3, to explore how persistence of the UB pattern in early November affects the following large-scale atmospheric circulation, under different sea ice conditions in the BK Seas. The motivation for the study was to reproduce and extend the results from P19, with a more realistic UB anomaly and another climate model than SC-WACCM4. Our results can be summarized as follows:

- The two models suggest that there is a window of opportunity for longer S2S prediction associated with a persistent UB pattern in fall (in this case, 2-week persistence in early November). Following the UB anomaly, a weakening of the polar vortex and negative NAO anomalies are found, which persist until mid-January. This means that there may be a 2-month window of predictability associated with persistent UB in November.
- The response to UB is greater under low sea ice conditions in the Barents Kara Seas, with negative NAO anomalies that persist longer in the season, compared to high sea ice conditions over BK. This means that greater NAO potential predictability following persistent-UB pattern is expected when SIC is low in the BK Seas, an interesting result—considering the observed sea-ice concentration decline—for S2S forecasting.
- When taken in isolation, the response to BK sea ice loss is secondary relative to the influence of UB. It induces almost no response in SC-WACCM4, and only a weak negative-NAO signal at the end of January in EC-Earth3. However, BK sea ice modulates the response to UB, not by increasing its persistence, but by influencing the persistence of the polar vortex warming that feeds back on the mean flow response in the North Atlantic.

The response to UB, and the weak impact of BK sea ice loss, support previous results from P19, and insights from the Polar Amplification Multimodel Intercomparison Project (PAMIP) experiments that explore the response to moderate Arctic sea-ice loss (D. M. Smith et al., 2022). We recognize that other studies have found a greater response to BK sea ice loss than we did, for example, Zhang et al. (2018), who also used SC-WACCM4. We note however that their forcing was stronger than ours, since they imposed future BK sea ice loss, throughout the whole winter. In contrast, our experiments only included observed anomalies from years 1988 and 2016, prescribed from November to mid-January. In this study, we only suggest that present-day November–December BK sea ice anomalies do not force a significant atmospheric response in early winter, but similar experiments with more persistent and larger BK sea ice anomalies throughout winter may show a larger response.

The novelty of the present study over P19 is that we find that the response to UB is robust in another atmospheric model, which is fundamentally different from SC-WACCM4, in terms of its dynamical core, numerical discretization, horizontal and vertical resolution, and physical parameterizations. Given the large number of degrees of freedom between the two models, in this study, we have not tried to attribute the difference in model responses to specifics of model properties or parametrizations. As mentioned earlier, given the difference in ensemble size, we cannot cleanly isolate what results from differences in models relative to the influence of internal variability. Our goal was mainly to show that the results from P19 can be reproduced in another atmospheric model with completely different characteristics. Additionally, the recent multimodel study by Xu et al. (2022) supports that the effect of UB we describe in this paper is simulated by state-of-the-art coupled climate models, lining up with the results from this study.

While we confirm the P19 finding that BK SIC anomalies alone have quite limited impact on the early winter atmospheric response, we find that they *modulate the response to UB* over the North Atlantic. Arctic sea ice is retreating at a fast rate (including BK sea ice), especially in fall and early winter. Therefore, our results suggest that persistent UB November events now may have a stronger impact on the atmosphere, compared to when

Arctic sea ice extent was greater. With continuing loss of Arctic sea ice, it is possible that the impact of UB will become stronger in the future, although a threshold may exist in how this effect works. It is also possible that other effects induced by climate change may counteract it. Whether the impact of UB becomes greater with reduced BK sea ice extent can be explored in climate scenarios, and in particular in the multi-model large ensemble archive (MMLEA, Deser et al., 2020), a valuable resource to investigate questions like this. Of note, SC-WACCM4 and EC-Earth3 underestimate eddy-mean flow interactions in the North Atlantic (D. M. Smith et al., 2022; Figure 6) as do all the models that were part of PAMIP. Therefore, it is possible that our experiments underestimate the real-world response to UB. This deserves attention by using an ensemble of model experiments with different amplitudes of eddy feedback, for example, from MMLEA or CMIP6. Another question, which is critical to S2S prediction, is associated with the minimum UB persistence required to induce a stratospheric response. In the present study, we imposed 2-week persistent UB anomalies. Will a 5-day event be enough to produce the slow-down of the stratospheric polar vortex and negative NAO? Since we focused on November UB events, it would also be interesting to assess the influence of UB events in winter, and check if they exert the same impact on the polar vortex/NAO.

Our findings are of interest to the field of S2S prediction, since we highlight November UB anomalies as a skillful predictor for the early mid winter NAO, and for the state of the polar stratosphere. We plan on further exploring what skill may be gained from using the UB as a predictor for the NAO/polar vortex in statistical models. This will provide a practical assessment of the potential benefit of using UB as a predictor in empirical forecast models, and/or of improving how UB and its associated teleconnections are represented in dynamical forecast models.

On a final note, our experiments were atmosphere-only simulations. A natural question to ask is whether an ocean-atmosphere coupled model may behave differently. Xu et al. (2022) show that the model mean state influences the strength of the UB teleconnection, so it is expected that a different model configuration with a different atmospheric basic state may exhibit different sensitivity to UB. In P19, UB experiments were replicated with a slab-ocean model to allow for sea ice melting and SST warming over BK. P19 did not find a strong impact of oceanic coupling, but the more realistic experiments we designed in the present study may be replicated with an interactive ocean, possibly fully coupled, to verify if it influences the large-scale atmospheric response to UB.

Appendix A

A1. Nudging of UB in SC-WACCM4

In the Ural domain (15°W/90°E; 45°N/80°N, surface to 300 hPa), the 3-dimensional temperature (T), the zonal (U) and meridional wind (V) and the surface pressure (PS) are prescribed to the model through a Newtonian relaxation. At each time step (t), the following term is added in the model prognostic equations of these variables:

$$X_{t+1} = X_t - k \times (X_t - X_{\mathrm{REF}}) \text{ with}$$

- X the prognostic variable computed by the model
- X_{REF} the value of the variable in the forcing field
- k the nudging coefficient that controls the strength of the relaxation

We use a value of $k = 0.05$, which corresponds to a 600 min (model time step of 30 min, divided by 0.05), or 10 hr, relaxation time. A small value of k is sufficient to successfully constrain the model, with PS, T, U, and V quickly converging to the target state, while retaining a little bit of high-frequency variability in the nudged domain. In order to include a buffer zone at the edges of the nudged domain, k decreases linearly from 0.05 to 0 over 10° in latitude along the horizontal, and three atmospheric levels along the vertical (full nudging at 500 hPa, linear decrease between 500 and 300 hPa, no nudging above 300 hPa). The buffer zones ensure a smooth transition from the nudged domain to the free atmosphere and avoid unrealistic steps in the controlled atmospheric variables. A linear decrease of the nudging coefficient, from 0.05 on 12 November, to 0 on 16 November, is also applied to ensure a gradual removal of the UB anomaly in the nudging domain.

A2. Nudging of UB in EC-Earth3

In the Ural domain (same as for SC-WACCM4), a 3-dimensional nudging is applied from the surface up to model level 55 (about 300 hPa) to temperature, vorticity, divergence, specific humidity, and surface pressure following a Newtonian relaxation similar to what implemented by WACCM4. Relaxation coefficient is $g = 0.1$, which corresponds to a 10 hr relaxation time for the first 12 days. Then the relaxation factor decreases daily to 0.075, 0.05,

and 0.025 and gets to 0 from the 16 November 00:00. A buffer zone is built using a sigmoid (logistic) function with growth rate $k = 1$, so that the nudging goes to zero in the horizontal in about 12° in both latitude and longitude. On the vertical, a sigmoid is built with $k = 2.5$, so that the nudging is zero at model level 51 (about 225 hPa). The buffer zones ensure a smooth transition from the nudged domain to the free atmosphere and avoid unrealistic steps in the controlled atmospheric variables.

Data Availability Statement

Model data from this study is available at https://doi.org/10.5281/zenodo.7470632 (Peings & Davini, 2022) and upon request to the authors.

Acknowledgments
The authors are grateful to the three anonymous reviewers who helped improving this manuscript. Y.P. and G.M. are supported by DOE Grant DE-SC0019407 and by the Department of Water Resources of California (Contract 4600013127). The authors are grateful for high-performance computing support from Cheyenne (https://doi.org/10.5065/d6rx99hx) provided by NCAR's Computational and Information Systems Laboratory, sponsored by the National Science Foundation, as well as from the National Energy Research Scientific Computing Center, a U.S. Department of Energy Office of Science User Facility. PD thanks ECMWF for providing computing time in the framework of the special projects SPITDAV2.

References

Bao, M., Tan, X., Hartmann, D. L., & Ceppi, P. (2017). Classifying the tropospheric precursor patterns of sudden stratospheric warmings. *Geophysical Research Letters*, *44*(15), 8011–8016. https://doi.org/10.1002/2017GL074611

Butler, A. H., Polvani, L. M., & Deser, C. (2014). Separating the stratospheric and tropospheric pathways of El Niño–Southern Oscillation teleconnections. *Environmental Research Letters*, *9*(2), 024014. https://doi.org/10.1088/1748-9326/9/2/024014

Butler, A. H., Sjoberg, J. P., Seidel, D. J., & Rosenlof, K. H. (2017). A sudden stratospheric warming compendium. *Earth System Science Data*, *9*(1), 63–76. https://doi.org/10.5194/essd-9-63-2017

Cohen, J., Furtado, J. C., Jones, J., Barlow, M., Whittleston, D., & Entekhabi, D. (2014). Linking Siberian snow cover to precursors of stratospheric variability. *Journal of Climate*, *27*(14), 5422–5432. https://doi.org/10.1175/jcli-d-13-00779.1

Cohen, J., Zhang, X., Francis, J., Jung, T., Kwok, R., Overland, J., et al. (2020). Divergent consensuses on Arctic amplification influence on mid-latitude severe winter weather. *Nature Climate Change*, *10*(1), 20–29. https://doi.org/10.1038/s41558-019-0662-y

Davini, P., Cagnazzo, C., & Anstey, J. A. (2014). A blocking view of the stratosphere-troposphere coupling. *Journal of Geophysical Research*, *119*(19), 11100–11115. https://doi.org/10.1002/2014JD021703

Davini, P., & D'Andrea, F. (2020). From CMIP3 to CMIP6: Northern Hemisphere atmospheric blocking simulation in present and future climate. *Journal of Climate*, *33*(23), 10021–10038. https://doi.org/10.1175/jcli-d-19-0862.1

de la Cámara, A., Birner, T., & Albers, J. R. (2019). Are sudden stratospheric warmings preceded by anomalous tropospheric wave activity? *Journal of Climate*, *32*(21), 7173–7189. https://doi.org/10.1175/jcli-d-19-0269.1

Deser, C., Lehner, F., Rodgers, K. B., Ault, T., Delworth, T. L., DiNezio, P. N., et al. (2020). Insights from Earth system model initial-condition large ensembles and future prospects. *Nature Climate Change*, *10*(4), 277–286. https://doi.org/10.1038/s41558-020-0731-2

Domeisen, D. I., Butler, A. H., Charlton-Perez, A. J., Ayarzagüena, B., Baldwin, M. P., Dunn-Sigouin, E., et al. (2020). The role of the stratosphere in subseasonal to seasonal prediction: 2. Predictability arising from stratosphere-troposphere coupling. *Journal of Geophysical Research: Atmospheres*, *125*, e2019JD030923. https://doi.org/10.1029/2019JD030923

Döscher, R., Acosta, M., Alessandri, A., Anthoni, P., Arneth, A., Arsouze, T., et al. (2021). The EC-Earth3 Earth System Model for the Climate Model Intercomparison Project 6. *Geoscientific Model Development*, *15*, 2973–3020. https://doi.org/10.5194/gmd-2020-446

Doss-Gollin, J., Farnham, D. J., Lall, U., & Mod, V. (2021). How unprecedented was the February 2021 Texas cold snap? *Environmental Research Letters*, *16*(6), 064056. https://doi.org/10.1088/1748-9326/ac0278

Fletcher, C. G., & Kushner, P. J. (2011). The role of linear interference in the Annular mode response to tropical SST forcing. *Journal of Climate*, *24*(3), 778–794. https://doi.org/10.1175/2010JCLI3735.1

Furtado, J. C., Cohen, J. L., & Tziperman, E. (2016). The combined influences of autumnal snow and sea ice on Northern Hemisphere winters. *Geophysical Research Letters*, *43*(7), 3478–3485. https://doi.org/10.1002/2016GL068108

Garfinkel, C. I., & Hartmann, D. L. (2008). Different ENSO teleconnections and their effects on the stratospheric polar vortex. *Journal of Geophysical Research*, *113*(D18), D18114. https://doi.org/10.1029/2008JD009920

Henderson, G. R., Peings, Y., Furtado, J. C., & Kushner, P. J. (2018). Snow-atmosphere coupling in the Northern Hemisphere. *Nature Climate Change*, *8*(11), 954–963. https://doi.org/10.1038/s41558-018-0295-6

Horton, D., Johnson, N., Singh, D., Swain, D. L., Rajaratnam, B., & Diffenbaugh, N. S. (2015). Contribution of changes in atmospheric circulation patterns to extreme temperature trends. *Nature*, *522*(7557), 465–469. https://doi.org/10.1038/nature14550

Huang, J., Tian, W., Zhang, J., Huang, Q., Tian, H., & Luo, J. (2017). The connection between extreme stratospheric polar vortex events and tropospheric blockings. *Quarterly Journal of the Royal Meteorological Society*, *143*(703), 1148–1164. https://doi.org/10.1002/qj.3001

Karpechko, A. Y., Charlton-Perez, A., Balmaseda, M., Tyrrell, N., & Vitart, F. (2018). Predicting sudden stratospheric warming 2018 and its climate impacts with a multimodel ensemble. *Geophysical Research Letters*, *45*(24), 13538–13546. https://doi.org/10.1029/2018GL081091

Kim, B. M., Son, S. W., Min, S. K., Jeong, J. H., Kim, S. J., Zhang, X., et al. (2014). Weakening of the stratospheric polar vortex by Arctic sea-ice loss. *Nature Communications*, *5*(1), 4646. https://doi.org/10.1038/ncomms5646

Kolstad, E. W., & Screen, J. A. (2019). Nonstationary relationship between autumn Arctic sea ice and the winter North Atlantic Oscillation. *Geophysical Research Letters*, *46*(13), 7583–7591. https://doi.org/10.1029/2019gl083059

Kretschmer, M., Cohen, J., Matthias, V., Runge, J., & Coumou, D. (2018). The different stratospheric influence on cold-extremes in Eurasia and North America. *npj Climate and Atmospheric Science*, *1*, 44. https://doi.org/10.1038/s41612-018-0054-4

Kuroda, Y. (2008). Effect of stratospheric sudden warming and vortex intensification on the tropospheric climate. *Journal of Geophysical Research*, *113*(D15), D15110. https://doi.org/10.1029/2007JD009550

Peings, Y. (2019). Ural blocking as a driver of early winter stratospheric warmings. *Geophysical Research Letters*, *46*(10), 5460–5468. https://doi.org/10.1029/2019GL082097

Peings, Y., Brun, E., Mauvais, V., & Douville, H. (2013). How stationary is the relationship between Siberian snow and Arctic Oscillation over the 20th century? *Geophysical Research Letters*, *40*(1), 183–188. https://doi.org/10.1029/2012GL054083

Peings, Y., & Davini, P. (2022). Model data from "Impact of Ural blocking on early winter climate variability under different Barents-Kara sea ice conditions". https://doi.org/10.5281/zenodo.7470632

Peings, Y., Labe, Z. M., & Magnusdottir, G. (2021). Are 100 ensemble members enough to capture the remote atmospheric response to +2°C Arctic sea ice loss? *Journal of Climate*, *34*(10), 3751–3769. https://doi.org/10.1175/jcli-d-20-0613.1

Petoukhov, V., Rahmstorf, S., Petri, S., & Schellnhuber, H. J. (2013). Quasiresonant amplification of planetary waves and recent Northern Hemisphere weather extremes. *Proceedings of the National Academy of Sciences of the United States of America*, *110*(14), 5336–5341. https://doi.org/10.1073/pnas.1222000110

Rayner, N. A., Parker, D. E., Horton, E. B., Folland, C. K., Alexander, L. V., Rowell, D. P., et al. (2003). Global analyses of sea surface temperature, sea ice, and night marine air temperature since the late nineteenth century. *Journal of Geophysical Research*, *108*(D14), 4407. https://doi.org/10.1029/2002JD002670

Siew, P. Y. F., Li, C., Ting, M., Sobolowski, S., Wu, Y., & Chen, X. (2021). North Atlantic Oscillation in winter is largely insensitive to autumn Barents-Kara sea ice variability. *Science Advances*, *7*, 31. https://doi.org/10.1126/sciadv.abg4893

Smith, D. M., Eade, R., Andrews, M. B., Ayres, H., Clark, A., Chripko, S., et al. (2022). Robust but weak winter atmospheric circulation response to future Arctic sea ice loss. *Nature Communications*, *13*(1), 727. https://doi.org/10.1038/s41467-022-28283-y

Smith, K. L., & Kushner, P. J. (2012). Linear interference and the initiation of extratropical stratosphere-troposphere interactions. *Journal of Geophysical Research*, *117*(D13), D13107. https://doi.org/10.1029/2012JD017587

Smith, K. L., Neely, R. R., Marsh, D. R., & Polvani, L. M. (2014). The Specified Chemistry Whole Atmosphere Community Climate Model (SC-WACCM). *Journal of Advances in Modeling Earth Systems*, *06*(3), 883–901. https://doi.org/10.1002/2014MS000346

Thompson, D. W. J., & Wallace, J. M. (2000). Annular modes in the extratropical circulation. Part I: Month-to-month variability. *Journal of Climate*, *13*(5), 1000–1016. https://doi.org/10.1175/1520-0442(2000)013<1000:AMITEC>2.0.CO;2

Tyrlis, E., Manzini, E., Bader, J., Ukita, J., Nakamura, H., & Matei, D. (2019). Ural blocking driving extreme Arctic sea ice loss, cold Eurasia, and stratospheric vortex weakening in autumn and early winter 2016–2017. *Journal of Geophysical Research: Atmospheres*, *124*(21), 11313–11329. https://doi.org/10.1029/2019jd031085

Vitart, F., & Robertson, A. W. (2018). The sub-seasonal to seasonal prediction project (S2S) and the prediction of extreme events. *npj Climate and Atmospheric Science*, *1*, 3. https://doi.org/10.1038/s41612-018-0013-0

Wang, L., Ting, M., & Kushner, P. J. (2017). A robust empirical seasonal prediction of winter NAO and surface climate. *Scientific Reports*, *7*(1), 279. https://doi.org/10.1038/s41598-017-00353-y

Woollings, T., Charlton-Perez, A., Ineson, S., Marshall, A. G., & Masato, G. (2010). Associations between stratospheric variability and tropospheric blocking. *Journal of Geophysical Research*, *115*(D6), D06108. https://doi.org/10.1029/2009JD012742

Xu, X., He, S., Zhou, B., Wang, H., & Outten, S. (2022). The role of mid-latitude westerly jet in the impacts of November Ural blocking on early winter warmer Arctic-colder Eurasia pattern. *Geophysical Research Letters*, *49*(16), e2022GL099096. https://doi.org/10.1029/2022GL099096

Yao, Y., Luo, D., Dai, A., & Simmonds, I. (2017). Increased quasi stationarity and persistence of winter Ural blocking and Eurasian extreme cold events in response to Arctic warming. Part I: Insights from observational analyses. *Journal of Climate*, *30*(10), 3549–3568. https://doi.org/10.1175/jcli-d-16-0261.1

Zhang, P., Wu, Y., Simpson, I. R., Smith, K. L., Zhang, X., De, B., & Callaghan, P. (2018). A stratospheric pathway linking a colder Siberia to Barents-Kara Sea sea ice loss. *Science Advances*, *4*(7), eaat6025. https://doi.org/10.1126/sciadv.aat6025